Journal of Structural Geology 32 (2010) 1996–2008

Contents lists available at ScienceDirect

Journal of Structural Geology

journal homepage: www.elsevier.com/locate/jsg

Late Pleistocene – Holocene ruptures of the Lima Reservoir fault, SW Montana

David J. Anastasio [a,*], Christina N. Majerowicz [a], Frank J. Pazzaglia [a], Christine A. Regalla [b]

[a] Lehigh University, Department of Earth and Environmental Sciences, 1 West Packer Avenue, Bethlehem, PA 18015-3001, United States
[b] Pennsylvania State University, Department of Geosciences, State College, PA 16802, United States

ARTICLE INFO

Article history:
Received 27 April 2009
Received in revised form
19 August 2010
Accepted 24 August 2010
Available online 11 November 2010

Keywords:
Normal faulting
Scarp diffusion model
Active tectonics
Basin and Range
Montana

ABSTRACT

Active tectonics within the northern Basin and Range province provide a natural laboratory for the study of normal fault growth, linkage, and interaction. Here, we present new geologic mapping and morphologic fault-scarp modeling within the Centennial Valley, Montana to characterize Pleistocene – Holocene ruptures of the young and active Lima Reservoir fault. Geologic relationships and rupture ages indicate Middle Pleistocene activity on the Henry Gulch (>50 ka and 23–10 ka), Trail Creek (>43 ka and ~13 ka), and reservoir (~23 ka) segments. Offset Quaternary deposits also record Holocene rupture of the reservoir segment (~8 ka), but unfaulted modern streams show that no segments of the Lima Reservoir fault have experienced a large earthquake in at least several millennia. The clustered pattern of rupture ages on the Lima Reservoir fault segments suggests a seismogenic linkage though segment length and spacing make a physical connection at depth unlikely. Trail Creek and reservoir segment slip rates were non-steady and appear to be increasing. The fault helps accommodate differential horizontal surface velocity measured by GPS geodesy across the boundary between the northern Basin and Range province and the Snake River Plain.

1. Introduction

Extension in the shallow crust is accommodated by the growth of normal fault segments (Dawers and Anders, 1995; McLeod et al., 2000; Walsh et al., 2003). The transfer of deformation within extensional systems can lead to seismogenic linkage (King et al., 1994; Stein, 1999; Di Bucci et al., 2006) or the propagation of ruptures to nearby faults due to co- or post-seismic reloading and relaxation of fault tips (Chery et al., 2001a, b; Kenner and Simons, 2005). These processes can result in a temporal clustering of seismic activity, which has been observed along several faults within the western United States (Lynch et al., 2003). Clustering of large magnitude earthquakes indicates non-steady, long-term slip rates. Understanding faults with long recurrence intervals requires combined paleoseismological data and the modern seismic record (Marco et al., 1996; Stickney and Lageson, 2002). A chronology of paleoruptures, fault rupture lengths, and fault displacements can inform assessments of seismic hazards and landscape evolution in tectonically active areas (Wells and Coppersmith, 1994). The actively deforming northern Basin and Range province in the western United States provides an excellent locality to study such normal fault development (Fig. 1).

In this study, we use geologic mapping to constrain the rupture length and segmentation of the Lima Reservoir fault and fault scarp morphologic modeling to reconstruct the timing of ancient surface ruptures along fault segments. A refined Quaternary stratigraphy of Centennial Valley provides a temporal framework to understand Pleistocene and Holocene ruptures and to assess the fault's development while accommodating deformation along the structural boundary between the Snake River Plain and the Basin and Range province. Models of fault scarp morphology estimate the time elapsed since surface rupture initiation and can provide a better estimate of fault slip rate than an estimate derived from dividing scarp offset by the age of the faulted horizon (e.g. Nash, 1980, 1986; Hanks et al., 1984; Mattson and Bruhn, 2001).

2. Geologic setting

2.1. Lima Reservoir fault

In southwest Montana, the Centennial Tectonic Belt is characterized by young, under filled grabens bounded by seismogenic normal faults of limited strike-length and throw (Stickney and Bartholomew, 1987). The Lima Reservoir fault is part of the Centennial Tectonic Belt, which extends westward from the Yellowstone eruptive center. (Fig. 1A). The Lima Reservoir fault outcrops as a series of discontinuous, south to southwest verging, extensional surface ruptures persisting for more than 24 km along

* Corresponding author. Tel.: +1 610 758 5117; fax: +1 610 758 3677.
E-mail addresses: dja2@lehigh.edu (D.J. Anastasio), cmajerowicz@gmail.com (C.N. Majerowicz), fjp3@lehigh.edu (F.J. Pazzaglia), cregalla@geosc.psu.edu (C.A. Regalla).

0191-8141/$ – see front matter © 2010 Elsevier Ltd. All rights reserved.
doi:10.1016/j.jsg.2010.08.012

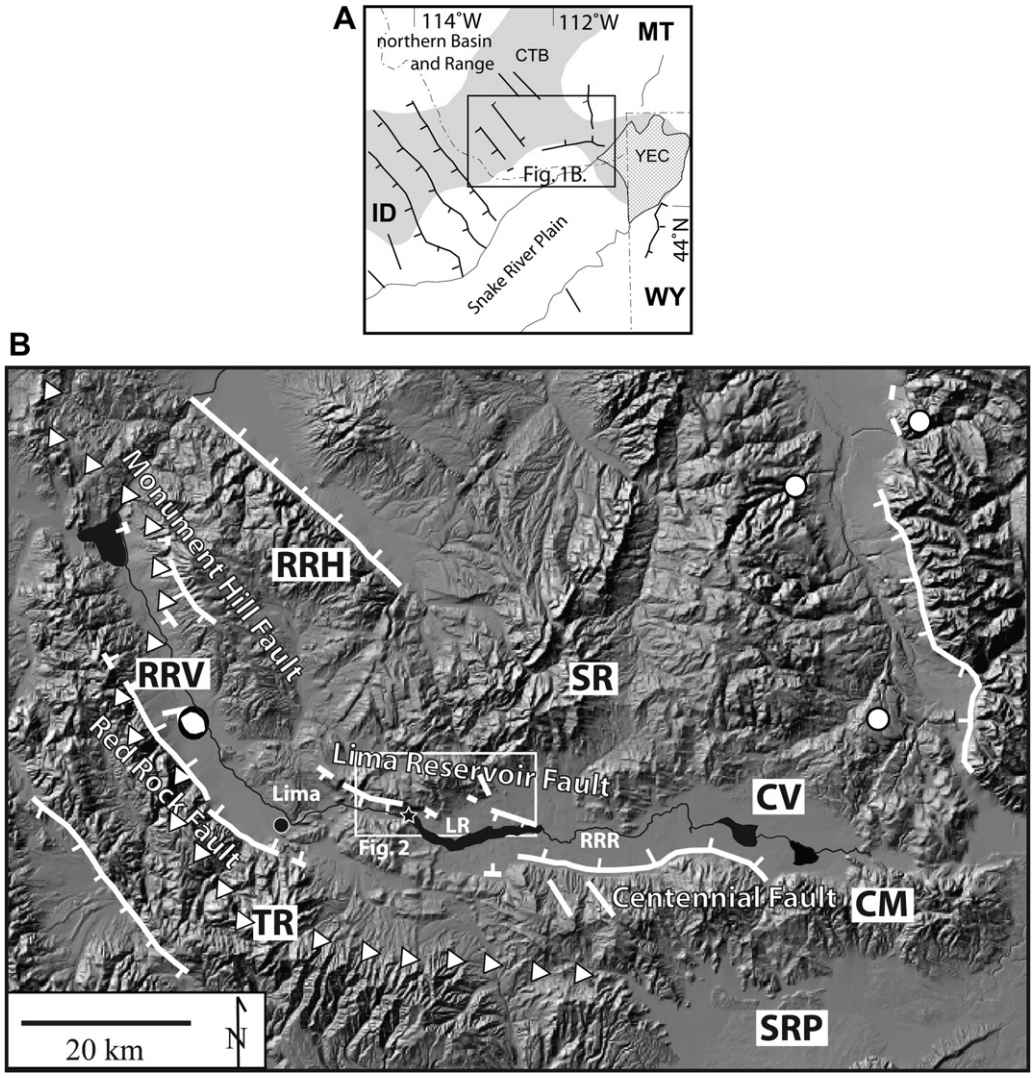

Fig. 1. Location map. A. Study location within the northern Basin and Range province, western United States showing major extensional faults. ID: Idaho, MT: Montana, WY: Wyoming, CTB: locus of Centennial Tectonic Belt seismicity shaded, YEC: Yellowstone eruptive center. B. Regional hill shaded DEM of SW Montana and NE Idaho locating faults discussed in text. White circles indicate locations of earthquake epicenters having magnitude 5.3 or larger. Focal mechanism solution is shown for the 1999 Kidd earthquake (Stickney et al., 2000). Triangles denote eastern extent of the Sevier thin-skinned thrust front. RRV: Red Rock Valley, SR: Snowcrest Range, TR: Tendoy Range, CV: Centennial Valley, CM: Centennial Mountains, SRP, Snake River Plain, RRR: Red Rock River, star indicates the location of the modern Lima Reservoir (LR) dam. Location of Fig. 2 shown.

the southern flank of the Laramide-style Snowcrest Range (Perry et al., 1988; Majerowicz, 2008; Fig. 1B). The fault includes the Henry Gulch, Trail Creek, and the reservoir segments (Fig. 2). In the adjacent Red Rock Valley, the Red Rock and Monument Hill faults are nearly coincident with the emergent Sevier thrust front (Harkins et al., 2005; Regalla et al., 2007) and in the Centennial Valley, the Centennial and Lima Reservoir faults border the Snowcrest Range suggesting that the locus and geometry of Quaternary-Holocene extensional faulting is inherited from earlier Sevier-Laramide contractional structures. The Centennial fault is a north-dipping normal fault, which together with the Lima Reservoir fault forms the Lima Reservoir graben defining the east-west trending Centennial Valley. The Centennial fault and the Lima Reservoir fault are listed as "Class A" faults by the U.S. Geologic Survey because of evidence of at least one rupture within the last 130 kyrs (Haller et al., 2000). Faults in northern Basin and Range province are less studied than to the south and may have displacement histories related both to regional extension and long-wavelength epeirogenic deformation related to passage of the Yellowstone eruptive center (Wegmann et al., 2007; Bartholomew et al., 2009).

2.2. Fault scarps

2.2.1. Henry Gulch segment

The Henry Gulch segment was recognized by Majerowicz et al. (2007), as a westward extension of the Lima Reservoir fault (e.g. Haller et al., 2000; Stickney et al., 2000) on the basis of faceted spurs, fault scarps, and offset Paleozoic units. The Lima Reservoir fault gradually changes orientation from east–west trending along the reservoir segment to northwest–southeast trending along the Henry Gulch segment to become strike-parallel with the Monument Hill fault further north (Fig. 1B). Where preserved, the Henry Gulch fault scarps are 2–5 m high. Along much of the trace, however, the fault scarps are covered by more recent mass flow deposits, which make them unsuitable for fault scarp morphological studies.

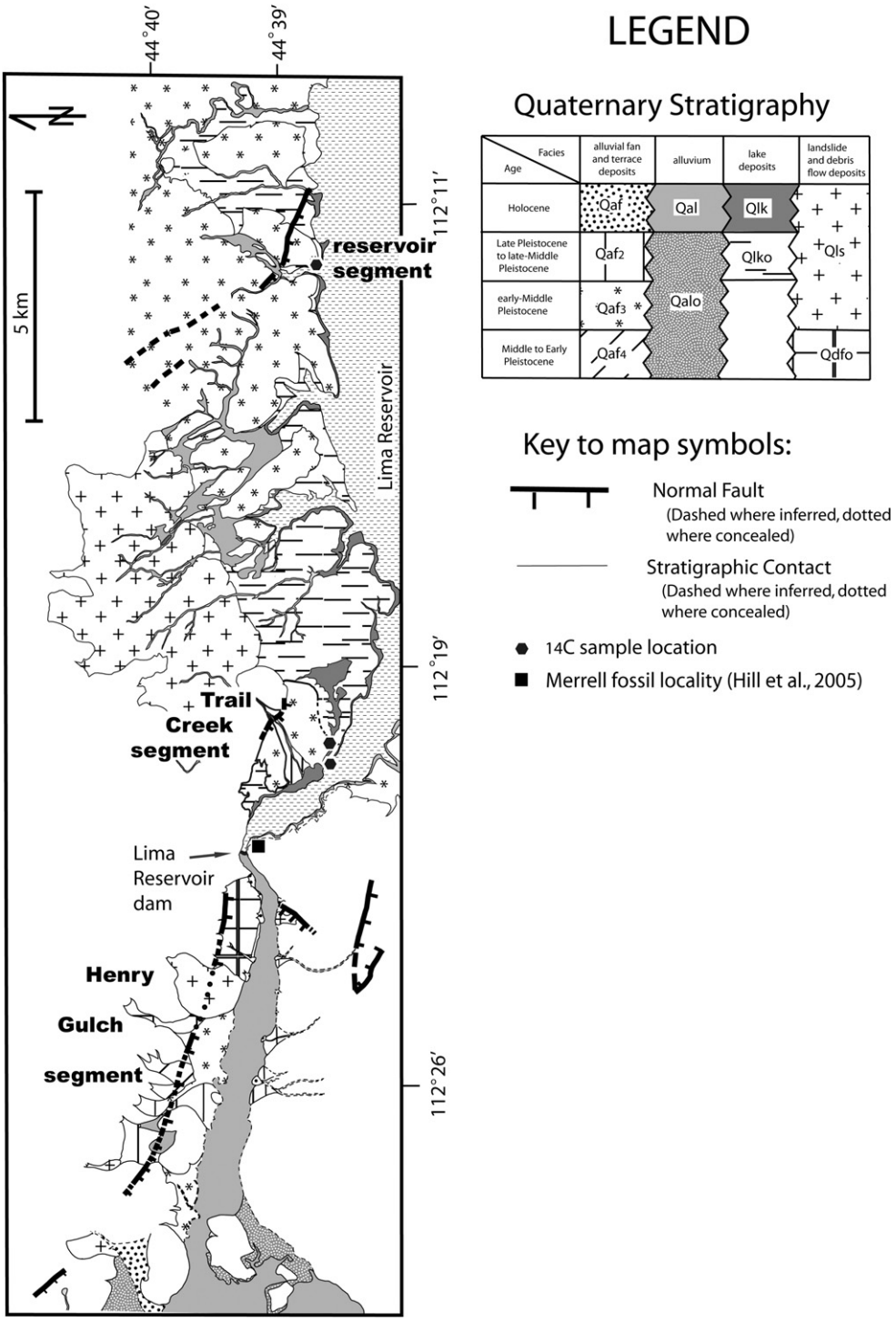

Fig. 2. Surficial Geologic map along the Lima Reservoir fault system. See Fig. 1 for map location. Tertiary and older units blank, see Majerowicz 2007, 2010 for bedrock geology.

Quaternary alluvium and debris flow deposits sourced primarily from the Tertiary Sixmile Creek Formation (fluvial and volcanoclastic deposits and basalt flows) form the valley walls of the Red Rock River near the site of the modern Lima Dam (Fig. 2) (Majerowicz et al., 2007, 2010). Mass movement of these materials into the Red Rock River Valley during the Pleistocene blocked the ancestral watershed creating a large lake in the Centennial Valley. The debris flow deposits head at faceted spurs along the Henry Gulch segment and the age of the littoral deposits (Hill et al., 2005) constrain a maximum age for a Middle Pleistocene rupture of the Henry Gulch segment of the Lima Reservoir fault. The extent of the Pleistocene pluvial lake is recorded by lacustrine and palaudal deposits that are incised by a paleo-shoreline, which provides a piercing point for Lima Reservoir fault displacement. The Henry Gulch segment offsets alluvial fan and older lacustrine deposits of Middle Pleistocene age but the fault does not cut Holocene alluvium (Fig. 2) (Majerowicz et al., 2007).

Table 1
Quaternary Stratigraphy of Centennial Valley. All Quaternary deposits are unconsolidated. Conventional 14C ages from Hill et al. (2005) and this study calibrated to calendar years before present (B.P.) using software available at http://www.radiocarbon.ldeo.columbia.edu/research/radiocarbon.htm, after Fairbanks et al. (2005), with 1σ uncertainties and 14C ages from Harkins et al. (2005), calibrated to calendar years B.P. with INTCAL98 following Stuiver et al. (1998), with 2σ uncertainties. OSL ages underlined with 1σ uncertainties. See text for further discussion. NA-Not Applicable, w-well, m-moderate, p-poorly [sorted], Ec-Eocene Challis Fm., Tsc-Tertiary Sixmile Creek Fm. Kabhc-Cretaceous Antonne Peak Fm., Beaverhead Gp., conglomerate Mbr. Ag-Precambrian Granitic Gneiss, Aq-Precambrian Quartzite. Supplemental Data for Geochronologic Samples from Centennial Valley includes stratigraphic correlation of dated samples, facies, lab sample numbers, type of material dated, conventional 14C ages, and literature references.

Age	Name Symbol	Description	Landscape Position	Vegetation	Soil Calcic Classification	14C Ages This Study	Published 1 Ages of Correlative Units A-E[a] and Qaf $_{1\text{-}4a}$[b]
Holocene-Late Pleistocene	Modern Alluvium Qal	w-p sorted fluvial silt, sand, and gravel	active channels and modern floodplain	NA	NA	NA	
early Holocene-Late Pleistocene	Older Alluvium Qalo	w-p sorted fluvial silt, sand, and gravel	preserved terraces above the modern floodplain	NA	Stage I	NA	
Holocene to early-Middle Pleistocene	Landslide and Debris Flow deposit Qls	p sorted, locally derived debris, often with hummocky topography	hillslopes to valley bottoms, mostly sourced from Tsc or Kabhc	NA	NA	NA	
Holocene	Modern Lake deposit Qlk	m-w sorted lacustrine silt and fine sand, beach gravels, no vegetation, seasonally submerged	flat topography adjacent to the modern reservoir	NA	NA	NA	
Late to late-Middle Pleistocene	Older Lake deposit Qlko	m-w sorted lacustrine silt, fine sand with occasional organic and gravel layers, loess cap 0.3-0.7 m thick with active dunes	surrounds and incised by Qlk deposits, interfingers with Qaf_2 deposits and overlies Qaf_3 deposits	sparse grass	NA	48350[c] 43855±673	B: 41696±646 B: 37874±310 B: >46000[c] C: 42000±4600
Holocene	Active Alluvial Fan deposit Qaf	p-m sorted silt to cobble alluvium, fan shape, wellpreserved bar and swale morphology	incised and inset into older fan deposits, active deposition close to modern reservoir	grass dominant	NA		Qaf_4: 1236±46 Qaf_{4a}: 3230±40 Qaf_{4a}: 3520±40 Qaf_{4a}: 4560±60
Late Pleistocene to late-Middle Pleistocene	Alluvial Fan deposit Qaf_2	p-m sorted silt to cobble alluvium, ~0.3 m loess cap, modified bar and swale morphology	0.5-1m above stream	moderate grass and sagebrush	Stage I+ to III-		D: 22942±156 D: 25885±167 D: 30048±685 Qft_3:10480±60
early-Middle Pleistocene	Alluvial Fan deposit Qaf_3	p-m sorted silt to cobble alluvium, modified fan shape, absence of bar and swale morphology, >0.3 m loess, some dunes	2-3m above stream	extensive grass, sagebrush, and cactus	II to III+	>30000[d]	A: 49350±1500[e] A: 63300±1,330 A: 58100±6,200
Middle to Early Pleistocene	Alluvial fan deposit Qaf_4	p-m sorted silt to cobble alluvium, lack of distinctive fan shape, or bar and swale morphology	higher elevations than and incised by younger fans	extensive grass, sagebrush, and cactus	II+ to III+		
Middle to Early Pleistocene	Older Alluvial fan deposit Qdfo	old, dissected alluvial deposits composed almost entirely of reworked Tsc Fm including clasts of Ec, Ag, Aq, poorly lithified, dark brown-red silt-loam soil, quartzite cobble lag on surface	isolated outcrops along Henry Gulch segment	extensive grass, sagebrush, and cactus	NA		

[a] Hill et al. (2005).
[b] Harkins et al. (2005).
[c] No uncertainty reported on conventional 14C age.
[d] Sample damaged during processing, age minimum.
[e] Conventional 14C age beyond radiocarbon calibration, conventional age reported.

2.2.2. Trail Creek and reservoir fault segments

Our rupture assessment of the Lima Reservoir fault focuses on two prominent sets of scarps, referred to as the Trail Creek and reservoir segments (Fig. 2). Along these two segments, the scarps are well exposed in the landscape and have well defined cross-cutting relations with dated Quaternary deposits. At the Trail Creek and reservoir scarps, Quaternary alluvial and lacustrine units are offset, however, the active stream channel deposits are not, nor has a knick point developed at or upstream of the fault trace. Scarp height varies along the fault, but is consistent within deposits of the same age. The Trail Creek scarp has a ground rupture length of ~1.2 km and the reservoir scarp has a rupture length of ~2.25 km. These fault scarps are separated by ~12.5 km (Fig. 2). The Middle Pleistocene shoreline along the reservoir segment presents a topographic scarp ~1 m high and where it crosses the scarp, it has a short fault-perpendicular trend exposing strike-parallel hanging wall and footwall cutoffs suggestive of down dip slip and extension.

2.3. Quaternary stratigraphy

We developed a Quaternary stratigraphy for Centennial Valley integrating inset and burial relationships, deposit surface morphology, soil calcic horizon development, and new and previously published radiometric 14C and optically stimulated luminescence (OSL) ages (Table 1 and Supplemental Data). Soil development was characterized in dug soil pits, ~1 m deep and along natural exposures, with particular attention afforded to the relative development of the calcic horizon (Gile et al., 1966; Ritter et al., 1993; Birkeland, 1999), which is known to be an age-dependent pedogenic feature in arid-land soils. The elevation of deposits above modern channels, the degree of fan dissection and surface bar and swale modification, and the type and abundance of vegetation were used to differentiate Quaternary units during mapping (Table 1). Correlation was made to dated deposits at the Merrell fossil locality (Hill et al., 2005) and to dated deposits in the nearby Red Rock Valley (Harkins et al., 2005) to establish a chronologic framework (Figs. 1 and 2, Table 1). At the Merrell locality, Hill et al. (2005) adopted a five unit Quaternary stratigraphy from A, the oldest, to E, the youngest. In Red Rock Valley, Harkins et al. (2005) defined four Quaternary fan-terrace units on the basis of sedimentology, stratigraphy, fan surficial morphology, a field-based soil chronosequence, and limited 14C dating.

2.3.1. Chronology of alluvial fan deposits

Qdfo-Qaf$_4$: We were able to distinguish and map five alluvial fan deposits along the Lima Reservoir fault. The two oldest fan deposits, Qaf$_4$ of fluvial origin and Qdfo debris flow facies, were not directly dated. Stratigraphic position based on inset and burial relationships and topographic position within Centennial Valley suggest an Early to Middle Pleistocene age for these deposits. Qdfo deposits were emplaced prior to 50.27 ka, the youngest possible age on the oldest sample of lacustrine unit A, which is the oldest unit at the Merrell locality (Hill et al., 2005).

Qaf$_3$: The oldest alluvial fan deposit that provides direct constraint on the paleoseismology of the Trail Creek and reservoir segments is Qal$_3$. Deposits of Qal$_3$ are truncated and inset by all younger alluvial fan and lacustrine deposits in Centennial Valley (Fig. 2). Shell material collected from Qaf$_3$ along the reservoir shore on strike to the dated Merrell locality horizons yielded a calibrated radiocarbon age of >30 ka (Table 1, Fig. 2). This sample suffered over-etching during laboratory analysis resulting in a depletion of usable material to date. Based on the samples position in the

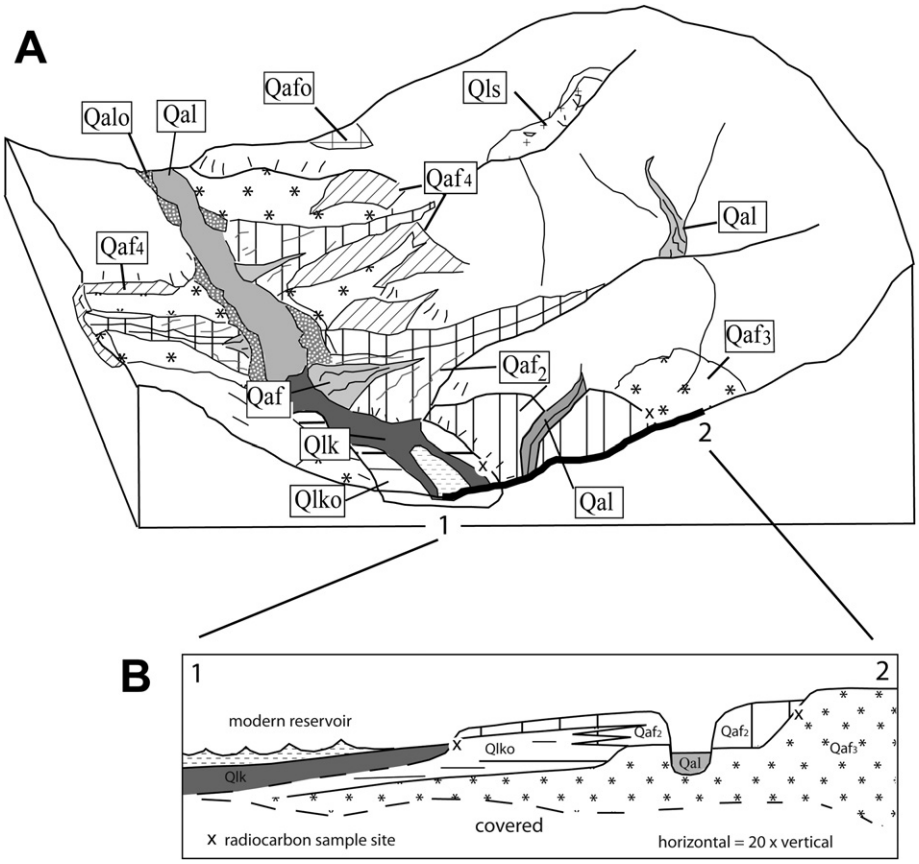

Fig. 3. Quaternary Stratigraphy. A. Schematic relationships of surfical units within the landscape. B. Simplified cross section along bold profile 1–2. See Fig. 2 for unit patterns.

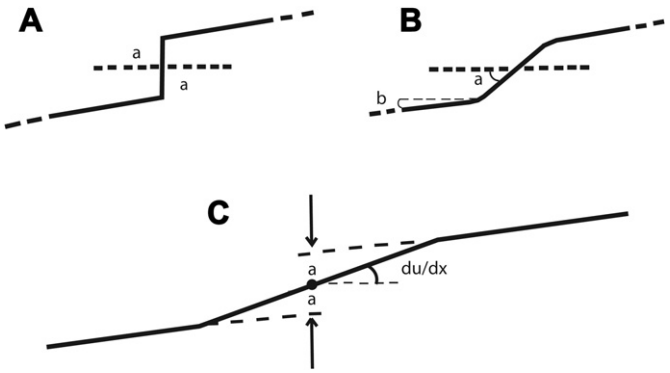

Fig. 4. Evolution of a fault scarp through time. A. Initially steep extensional fault scarp is degraded by gravity driven processes for several centuries until the angle of repose is reached. B. Diffusive processes then dominate scarp evolution. This profile shape serves as the initial condition for morphologic modeling. C. Measured modern fault scarp profile. Profile shape continues to evolve by diffusion to match the background slope (after Hanks, 2000).

landscape and the amount of pedogenic carbonate in the host sediment it is most likely radiocarbon dead and therefore, >50 ka. Hill et al. (2005), report OSL ages of 58.1 ± 6.2 ka and 63.3 ± 13.3 ka from unit A, the stratigraphic equivalent to the offset Qaf_3 deposits. We conservatively bracket the age of Qaf_3 as being older than the youngest 14C age on an inset Qlko deposit (Fig. 3) and as young as the oldest OSL age on unit A plus the uncertainty at 43.18–76.60 ka or 59.89 ± 16.71 ka.

Qaf_2: Due to the morphologic and sedimentological similarities between Qaf_3 and Qaf_2 deposits, the relative landscape position (elevation above the modern stream channel) was used as the most distinguishing characteristic during mapping (Table 1). We were not able to directly date Qaf_2 in Centennial Valley but fans with similar characteristics are dated ~20 –10.42 ka in Red Rock Valley (Harkins et al., 2005). Qaf_2 correlates to unit D of Hill et al. (2005), which has a minimum calibrated radiocarbon age of 22.94 ± 0.16 ka (Table 1). Dated unit D samples are from a debris flow therefore the youngest dated sample provides a maximum age for the deposit. In Centennial Valley, unit Qaf2, is assigned an age of 16.68 ± 6.26 ka, a range that encompass the correlated dated material.

Qaf-Qal: The youngest alluvial fans within Centennial Valley are actively depositing material close to the modern reservoir. The Qal and Qaf deposits are not cut by the Lima Reservoir fault. The active fans and associated modern stream channels are inset into and dissect all older fan deposits. In texture, stratigraphic position, and age, Qaf and Qal are Holocene deposits correlative to unit E of Hill et al. (2005) and units Qaf_4 and Qaf_{4a} of Harkins et al. (2005). Calibrated 14C ages for Red Rock Valley samples are between 1.236 ± 46 (Qaf_{4a}) and 4.560 ± 60 (Qaf_4) ka (Table 1).

2.3.2. Lake deposits

Qlko-Qlk: Ancient lake deposits include stratified silt and sand and freshwater limestone outcropping in natural bluffs surrounding the modern Lima Reservoir. In Centennial Valley, shells from Qlko yielded calibrated radiocarbon ages of 43.86 ± 0.67 ka and 48.35 ka (Table 1). Field relations demonstrate that the deposit interfingers with the lower to middle Qaf_2 section and overlies Qaf_3 (Fig. 3). In texture, stratigraphic position, and age, this older lake deposit is correlative to units B and C of Hill et al. (2005). Using all available geochronology (Table 1), we adopt a conservative age range of 46.60–16.26 ka or 31.43 ± 15.17 ka for

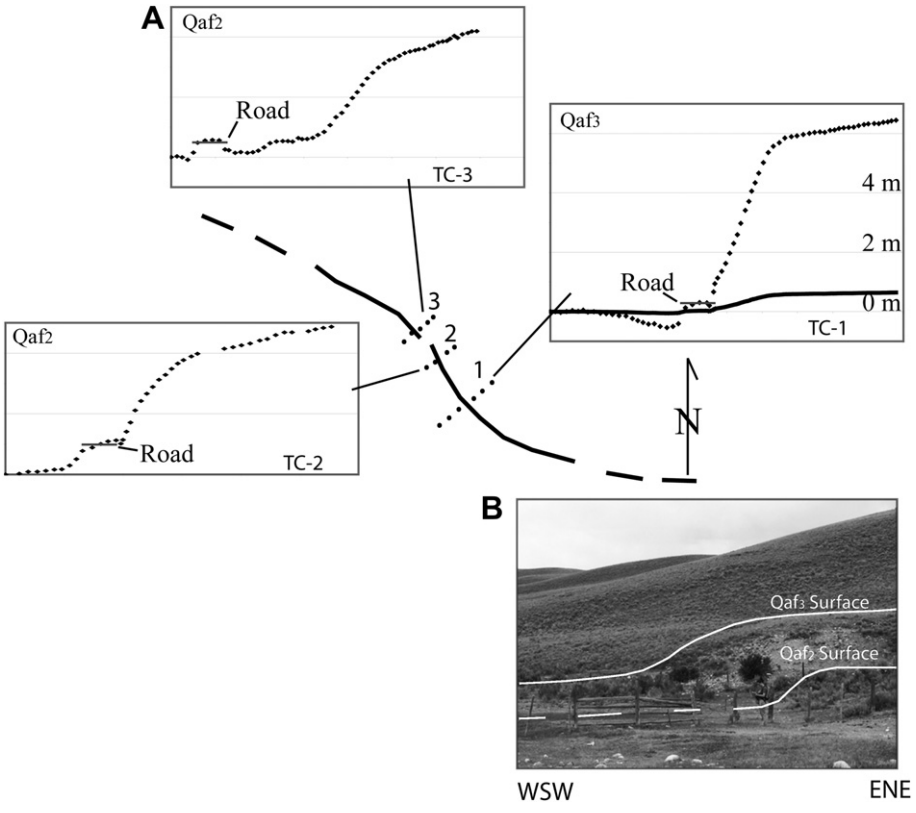

Fig. 5. Trail Creek segment scarp profiles. A. Measured profiles along the Trail Creek scarp with ~10:1 vertical exaggeration. Profile locations keyed to sketch of fault trace. Profile lengths are: 1 = 100 m, 2 = 60 m, 3 = 80 m. The offset Quaternary surface is indicated on each graph. Graph TC-1 shows the topographic profile without vertical exaggeration as solid black line. The location of a maintained dirt road is indicated on each profile. B. Field photograph of the Trail Creek scarp.

Qlko in Centennial Valley. The younger lake deposit, Qlk, is Holocene and accumulating in the portion of the landscape that is seasonally covered by the modern reservoir.

3. Fault scarp morphologic modeling

Fault scarps are a topographic break in slope created by a rupture that extends to the land surface. Within the Basin and Range province, Wells and Coppersmith (1994) reported that a magnitude M 6.5 earthquake is required to rupture the surface. Recent earthquakes in Red Rock Valley with magnitudes up to M 5.6 did not rupture the surface (i.e. 1999 Red Rock Valley, Fig. 1B). The Lima Reservoir fault scarps are evidence of larger prehistoric earthquakes in Centennial Valley that precede the modern seismic record. The reservoir scarp offsets Qlko (31.43 ± 15.17 ka) and Qaf_3 (59.89 ± 16.71 ka) surfaces and the Trail Creek scarp offsets Qaf_2 (16.68 ± 6.26 ka) and Qaf_3 (59.89 ± 16.71 ka) surfaces, but neither offset the modern alluvium (Majerowicz et al., 2007, 2010). Therefore, map relationships bracket the time of last rupture of the Lima Reservoir fault to at least late-Middle Pleistocene, the age of unit Qaf_2.

To better establish ages and patterns of fault rupture, we measured topographic profiles and modeled the morphology of fault scarp degradation (e.g. Wallace, 1977; Avouac, 1993; Hanks, 2000). When scarps degrade by surface processes, the evolution of the scarp profile can be modeled as a diffusive process. Calibration of diffusivity, parent materials, and scarp shape can be inverted to determine the scarp age or time of rupture. Given enough time, a scarp will degrade to match the background slope of the hanging wall and footwall (Fig. 4). This view of fault scarp evolution assumes that the rate of sediment movement downslope is transport limited, the material is unconsolidated with no cohesion, and movement is proportional to the local slope (Wallace, 1977; Nash, 1980). These assumptions are valid in the semi-arid environment of the northern Basin and Range province.

The surface offset of a geomorphic marker records the fault throw and its rate of vertical displacement provides good estimate of fault slip rate for steep dip-slip faults like those in the Basin and Range province. In the case of the 60° dipping principal rupture plane of the Lima Reservoir fault (Bartholomew et al., 2002) with dip-slip motion the throw is 87% of the fault slip. The results from our scarp morphologic models provide an estimate of the rate of fault throw and a good approximation of the fault slip. We adopt common usage and refer to the throw rate as fault slip rate to be consistent with the literature (e.g. Nash, 1986; Hanks, 2000).

The surface offset is generally assumed to have occurred during a single rupture in scarp degradation studies, though this behavior is often not the case. The single-rupture assumption is valid when fault ruptures are less frequent than the scarp decay time. Both the Trail Creek and reservoir segments offset older landscape surfaces more than younger ones (Figs. 5 and 6), suggesting that the residual topographic scarps resulted from multiple ground-rupturing events. Several offset paleosols in loess from an exploratory trench across the reservoir segment support a protracted rupture history for the Lima Reservoir fault (Bartholomew et al., 2002). Therefore, in addition to traditional single-rupture modeling (SlopeAge II

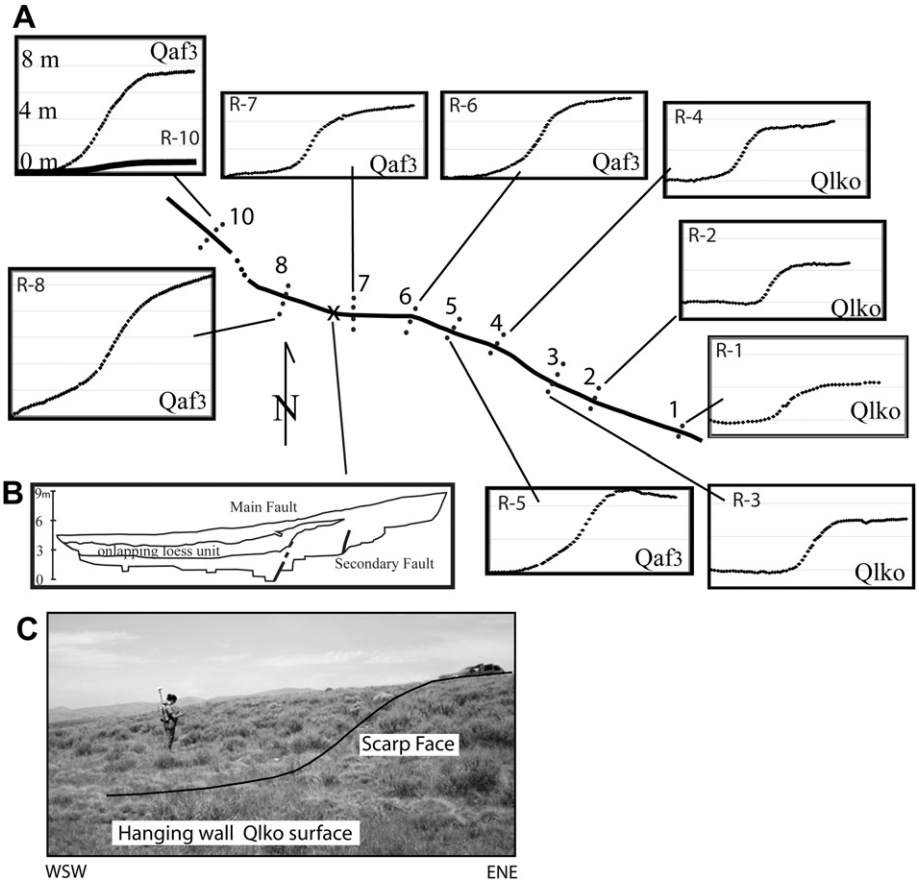

Fig. 6. Reservoir segment scarp profiles. A. Measured profiles along the reservoir scarp with ~10:1 vertical exaggeration. All profiles use the same vertical scale, labeled on profile R-10. Profiles are 100 m in length except for profile R-1 of 60 m and profiles R-8 and R-10 of 110 m. The offset Quaternary surface is indicated on each graph. B. Simplified sketch (reversed) of the reservoir segment trench after Bartholomew et al. (2002). C. Field photograph of the reservoir scarp, looking westward from near its midpoint.

program, Nash, 2005), we modeled the scarps as continuously forming and degrading during constant fault slip (e.g. Mattson and Bruhn, 2001). The results from the single-slip and constant-slip models are internally consistent and are both used in reconstructing the paleorupture history of the Lima Reservoir fault. Single-slip models are most common in the literature (e.g. Wallace, 1977; Nash, 1980; Avouac, 1993; Hanks, 2000; Regalla et al., 2007) so they allow us to compare the traditional single-slip model results to those from our constant-slip methodology. Single-slip models (e.g. Nash, 2005) utilize the entire scarp profile to calculate the age of rupture. Eroded material from up-slope collects at the scarp base, which is also susceptible to differential loess accumulation banking up against the scarp. Both processes reduce the scarp dip and thus single-slip models provide a maximum fault rupture age. To avoid the complications inherent in the full scarp profile and to complement the single-slip rupture age estimates, we used only the upper half of the exposed footwall scarp in our constant-slip models. As a consequence, our constant-slip models tend to provide a minimum rupture age estimate, which have smaller age uncertainties (Tables 2A and 2B).

Regalla et al. (2007) determined a diffusivity constant, k equal to 1.257 m^2/kyr, using similarly unconsolidated fluvial terrace deposits of known age within the neighboring Red Rock Valley (Qft_2 and Qft_3 of Harkins et al., 2005) offset by the Red Rock fault. The Red Rock Valley diffusion constant falls within the range of published k values for the northern Basin and Range province (Pierce and Coleman, 1986; Nash, 1984), as well as those calculated for Lake Bonneville, Utah shoreline scarps (Mattson and Bruhn, 2001). We generated overlapping rupture ages from both single-slip and constant-slip models of nearby scarp profiles across sands, gravels, and cobbles of Qaf_3 alluvial fan deposits and sands and silts of the Qlko lacustrine deposit along the reservoir scarp providing us with a rationale to hold k constant for all of our reported model runs.

3.1. Single-Slip scarp models

Nash (1986, 2005) treats fault scarp degradation as a linear diffusion process described as

$$\frac{du}{dx} = k\frac{d^2u}{dx^2} \tag{1}$$

where u is surface elevation and x is horizontal position along the profile in meters, both with respect to the profile midpoint, and k is the diffusion constant in m^2/kyr. The diffusion model is applied to an initial scarp profile with half throw offset a in meters between the projected footwall and hanging wall surfaces, a regional slope or undisturbed footwall fan slope b, and an initial scarp slope α, obtained directly from the measured profiles (Fig. 4). Forward modeling solved for time T on the criteria of a root-mean-square (RMS) best fit between the modeled and measured profiles. Values for a, b, and du/dx were calculated for each profile from regression lines constructed through the reduced scarp face and the footwall fan surface data. For these models, the assigned, initial profile was incrementally degraded with individual time steps, T, of 20 years in 100-year increments with $k = 1.257$ m^2/kyr. After multiple trial runs with various combinations of input variables including diffusion constant, fault midpoint, and slip rate, additional model runs were completed to determine a lowest RMS best fit value for each profile with α, the initial input for scarp face angle, varied between 30° and 40°. We chose the initial scarp slopes because a scarp face degrades to the angle of repose of unconsolidated alluvium over a period of a few centuries in response to gravity driven rather than diffusive processes (Wallace, 1977; Bucknam and Anderson, 1979). The modeled ages are reported as mean rupture age in thousands of years $\pm 1\sigma$ standard deviation (Table 2A and B).

3.2. Constant-slip scarp models

Mattson and Bruhn (2001) applied non-linear modeling to multiple-event scarps approximated by accumulating surface offset at a constant rate from an initial horizontal surface. The constant slip-rate model is an analytic solution that assumes that the slip occurs as incrementally small instantaneous vertical displacements (<1 mm), which continuously degrade by diffusion. The constant-slip–rate equation:

$$u(x,t) = (a+At)erf\left(\frac{x}{2\sqrt{kt}}\right) + \frac{Ax^2}{2k}\left[erf\frac{x}{2\sqrt{kt}} - \mathrm{sgn}(x)\right] + \frac{Ax}{k}\sqrt{\frac{kt}{\pi}}e^{(-x^2/4kt)} + bx \tag{2}$$

Table 2A
Modeled rupture ages for each profile across the Trail Creek and reservoir segments of the Lima Reservoir fault. For each profile rupture age is reported as the mean age of rupture of all runs for both the single-slip and constant-slip model results with 1σ standard deviation. Slip (throw) rate calculated for each offset and rupture age pair and averaged for each fault segment.

Profile Number	Ruptured Unit	Throw (m)	Modeled Age (ka) Single-Slip	Modeled Age (ka) Constant-Slip	Slip Rate (m/ka) Single-Slip Age	Slip Rate (m/ka) Constant-Slip Age
Trail Creek Segment						
TC-1	Qaf_3	5.64	12.57±1.72	15.3±0.47	0.45±0.46	0.37±0.01
TC-2	Qaf_2	3.09	6.10±0.54[a]	7.00±0.00[a]		
TC-3	Qaf_2	2.59	13.78±1.45	9.00±0.41	0.19±0.02	0.29±0.02
segment mean			13.18±2.38	12.20±0.67	0.32±0.24	0.33±0.01
Reservoir Segment						
R-1	Qlko	2.26	9.75±4.17	5.50±0.41	0.23±0.14	0.41±0.04
R-2	Qlko	2.61	11.12±4.21	9.30±0.47	0.23±0.09	0.28±0.02
R-3	Qlko	2.84	18.22±3.39	5.30±0.47	0.16±0.03	0.54±0.05
R-4	Qlko	2.50	7.38±0.65	2.30±0.47	0.34±0.03	1.09±0.23
mean eastern sector	Qlko	2.25±0.18	11.62±6.08	5.60±1.34	0.24±0.07	0.58±0.08
R-5	Qaf_3	3.42	25.30±6.51	5.30±0.47	0.14±0.06	0.64±0.06
R-6	Qaf_3	4.73	30.40±6.78	17.5±1.34	0.16±0.04	0.27±0.02
R-7	Qaf_3	3.25	26.33±3.22	14.17±1.77	0.12±0.02	0.23±0.03
R-8	Qaf_3	5.18	28.18±7.94	17.30±1.25	0.18±0.05	0.30±0.02
mean central sector	Qaf_3	4.39±0.19	28.30±10.74	16.32±2.67	0.15±0.04	0.27±0.02
R-10	Qaf_3	3.30	40.10±2.31	19.00±0.82	0.08±0.01	0.17±0.01
Qaf_3 rupture mean	Qaf_3	3.98±0.91	30.06±4.19	14.65±2.59	0.14±0.03	0.32±0.03
Rerervoir segment mean					0.18±0.05	0.44±0.05

[a] Rupture age suspect because of anthropogenic scarp modification, therefore, excluded from mean rupture age, slip rates not calculated.

defines a as the half throw, b as the background slope, A as the half-slip (throw) rate, k as the diffusivity constant and t as time. The sign function, sgn, returns +1 or −1 based on the sign of the argument, x is the horizontal position along the profile and u is the modeled height associated with that horizontal position at a specific time. As with the single-slip modeling a and b are calculated directly from the measured profiles and kept constant for all model runs for each individual profile. Modeled rupture ages are particularly sensitive to the half-scarp offset a, which was carefully determined from measured profiles. The diffusion constant k was kept constant, 1.257 m^2/kyr for all model runs. All of constant-slip models were run to simulate 20–40 kyr of scarp degradation.

MatLab 7.4 was used for the constant–slip calculations using a custom code (provided as Supplemental Material) that allowed for the input and manipulation of individual variables for testing model sensitivity. The measured scarp profile was input and eq. (2) was used to forward model an initial planar surface to a final profile in 1-kyr time steps until the specified maximum time span. At each time step, a model profile was created and an RMS best fit value was calculated based on the residuals between model and observed elevations along the topographic profile. This approach creates multiple profiles that act as snapshots for profile evolution through time based on assigned variables. The time associated with the smallest RMS value was chosen as the estimated time since rupture initiation at the location. After trial and error to explore model sensitivity to various input parameters, each profile was modeled an additional 3–7 times to produce a best fit, low RMS value from which a fault initiation age and uncertainty estimates were derived.

4. Results

4.1. Fault scarp profiles

Fault scarp morphologic profiles were collected using paired mobile and local base station Trimble 5700 GPS receivers in a post-processed kinematic survey. Data collection protocols employed with the instruments provides centimeter-scale accuracy in horizontal position and ~10-cm accuracy in elevation. Along the Trail Creek segment, three fault-scarp profiles were modeled. Two profiles traverse offsets the Qaf_2 surface and one profile traverses the offset Qaf_3 surface (Fig. 5). The reservoir scarp was profiled along nine transects with four crossing the Qlko surface and five crossing the Qaf_3 surface (Fig. 6). Each profile was oriented perpendicular to the fault scarp and included the scarp face and offset fan surface. Profile spacing was chosen to include the maximum and minimum displacement of the fault scarp as well as all offset surficial units. Care was taken to extend the profile to include the background slope and to minimize the effects of anthropogenic disturbances.

Fault throw along the Lima Reservoir fault varies both as a function of position along the scarp and as a function of the age of the offset surface (Table 2A). Along the Trail Creek scarp, the throw across Qaf_2 averaged 2.84 ± 0.35 m, whereas, the throw across the Qaf_3 surface was 5.64 ± 0.10 m (Fig. 5). Along the reservoir scarp, the throw on Qlko averaged 2.55 ± 0.24 m and the throw of Qaf_3 was 4.71 ± 1.36 m. The reservoir segment trench exposed a buried scarp ~2.3 m high beneath the trace of the exposed fault (Bartholomew et al., 2002) (Fig. 6), similar to the throw on the exposed offset Qlko surface.

Table 2B
Summary of Pleistocene – Holocene rupture ages and slip rates for the Lima Reservoir fault.

Fault Segment	Offset Unit(s)	Strike Length (m)	Rupture Age (ka)	Slip Rate (m/kyr)
Henry Gulch	bedrock, Qdfo, Qaf_4, Qaf_3, Qaf_2	10000	> 50, 23 - 10	?
Trail Creek	Qaf_2, Qaf_3	1200	> 43, 12.66±1.48	0.32±0.13
central reservoir R-6, R-7, R-8	Qaf_3	750	23.31±6.70	0.19±0.06
eastern reservoir R-1, R-2, R-3, R-4	Qlko	900	8.11±4.10	0.28±0.14
reservoir segment	Qaf_3, Qlko	2200	~23, ~8	0.31±0.05
Lima Reservoir Fault	Qaf_2, Qaf_3, Qlko	24600	>50, ~23, ~13, ~8	0.31±0.06

4.2. Modeling results

4.2.1. Trail Creek scarp ruptures

Profile TC-1 crossed the Trail Creek scarp on the Qaf_2 surface on the west side of the creek and yielded a single-slip rupture age of 13.78 ± 1.45 ka (Fig. 7, Table 2A). Nearby profile TC-3 crossed Qaf_3 and yielded a single-slip age of 12.57 ± 1.72 ka. These rupture ages are nearly identical, although the throw is twice as great across the older Qaf_3 surface suggesting the Trail Creek fault has slipped more than once. The constant-slip rupture age along the western profile crossing Qaf_2 is 9.00 ± 0.41, a bit younger than the single-slip simulation. The profile across Qaf_3 yielded a constant-slip rupture age of 15.30 ± 0.50 ka, within the uncertainty of the single-slip model result. Profile TC-2 on the east side of the creek across the ruptured Qaf_2 surface produced much younger ages, 6.10 ± 0.54 ka from single-slip and 7.00 ± 0.00 ka from the constant-slip algorithm. Road construction adjacent to the Trail Creek segment modified the eastern Qaf_2 scarp face (TC-2, Fig. 5), such that the profile is unusually downwards rather than upwards steepening. Because anthropogenic steepening of the scarp results in an unreliable and artificially younger modeled age, we rely only on the concave up western profiles to assess the rupture age of the Trail Creek segment (Table 2A and B). Profile TC-1 crossing Qaf_3 deposits was also impacted by road construction but to a lesser extent and

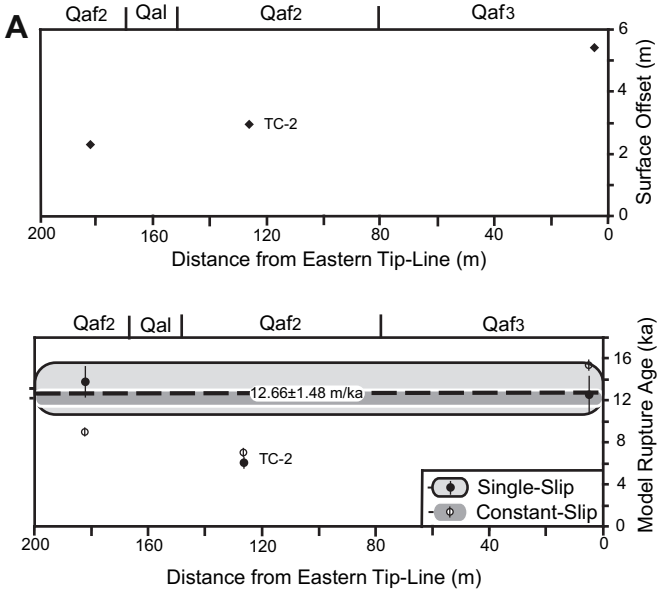

Fig. 7. Surface offset (fault throw) and modeled rupture ages along the Trail Creek segment of the Lima Reservoir fault. Offset Quaternary units are indicated. A. Throw measured at profile sites along the fault trace; distance is measured from the eastern tip-line. B. Modeled rupture age as a function of position with 1σ uncertainties. Shaded areas are rupture age means by model with 2RSE, the mean value is marked.

only at the very base of the scarp so these data were not discarded. The rupture age of the Trail Creek segment is taken to be 12.66 ± 1.48 m/ka, the average from the offset Qaf_3 and Qaf_2 surfaces determined by both model methods from profiles TC-1 and TC-3 (Fig. 7).

4.2.2. Reservoir scarp ruptures

The rupture ages across the reservoir segment generally fall into one of two groups (Fig. 8). The youngest rupture, determined from the ~900 m long eastern sector defined by profiles R-1, R-2, R-3, and R-4 across the offset Qlko surface, yielded a single-slip age of 11.62 ± 6.08 ka and constant-slip age of 5.60 ± 1.34 for an average rupture age of 8.11 ± 4.10 ka. The ~750 m long central sector is defined by profiles R-6, R-7, and R-8, which crossed the ruptured Qaf_3 surface and yielded a single-slip age of 28.30 ± 10.74 ka, a constant-slip age of 16.32 ± 2.67 ka, and an average rupture age of 22.31 ± 6.70 ka. The results from single-slip and constant-slip models of profiles R-5 and R-10 were more divergent and in contrast to the results from the other profiles, there was no overlap in the bracketed rupture age range, therefore no conclusion was drawn from these profiles. For all the profiles crossing the reservoir scarp, constant-slip modeling estimated younger rupture ages with smaller uncertainties than the results from single-slip models (Table 2A and B).

4.3. Slip rates

Minimum long-term slip rates were calculated for the Lima Reservoir fault system by dividing the surface throw along the Trail Creek and reservoir segments by the age of the oldest offset deposit, Qaf_3 in both cases. The reservoir segment offsets the Qaf_3 surface with an average throw of 4.71 ± 1.36 m and at the Trail Creek segment Qaf_3 offset is 5.64 m with a measurement of uncertainty of ±0.10 m. The age range of the Qaf_3 deposit is 59.89 ± 16.71 ka. The minimum long-term slip rate of the Trail Creek segment is 0.09 ± 0.03 m/kyr and the minimum slip rate of the reservoir segment is 0.08 ± 0.04 m/kyr. The minimum slip rate calculations assume that slip initiation was contemporaneous with the age of the offset surface. A nearly constant-slip rate of 0.14 ± 0.01 would satisfy the field relations but rates half to twice as fast would be consistent with at least one scarp offset (Fig. 9A). Slip rates between 0.05 m/kyr and 1.00 m/yr were explored during modeling, but slip rates of 0.22–0.26 m/kyr produced the best model results, so were used to determine the age of rupture during model simulations.

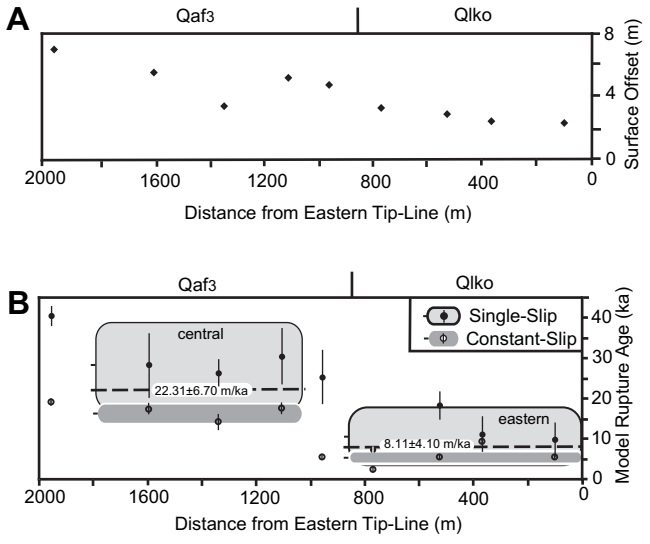

Fig. 8. Surface offset (fault throw) and modeled ages along the reservoir segment of the Lima Reservoir fault system. Offset Quaternary units are indicated. A. Throw measured at profile sites along the fault trace; distance is measured from the eastern tip-line. B. Modeled rupture age as a function of position with1σ uncertainties. Shaded areas are rupture age means for the central and eastern sectors by model with 2RSE, the mean value is marked.

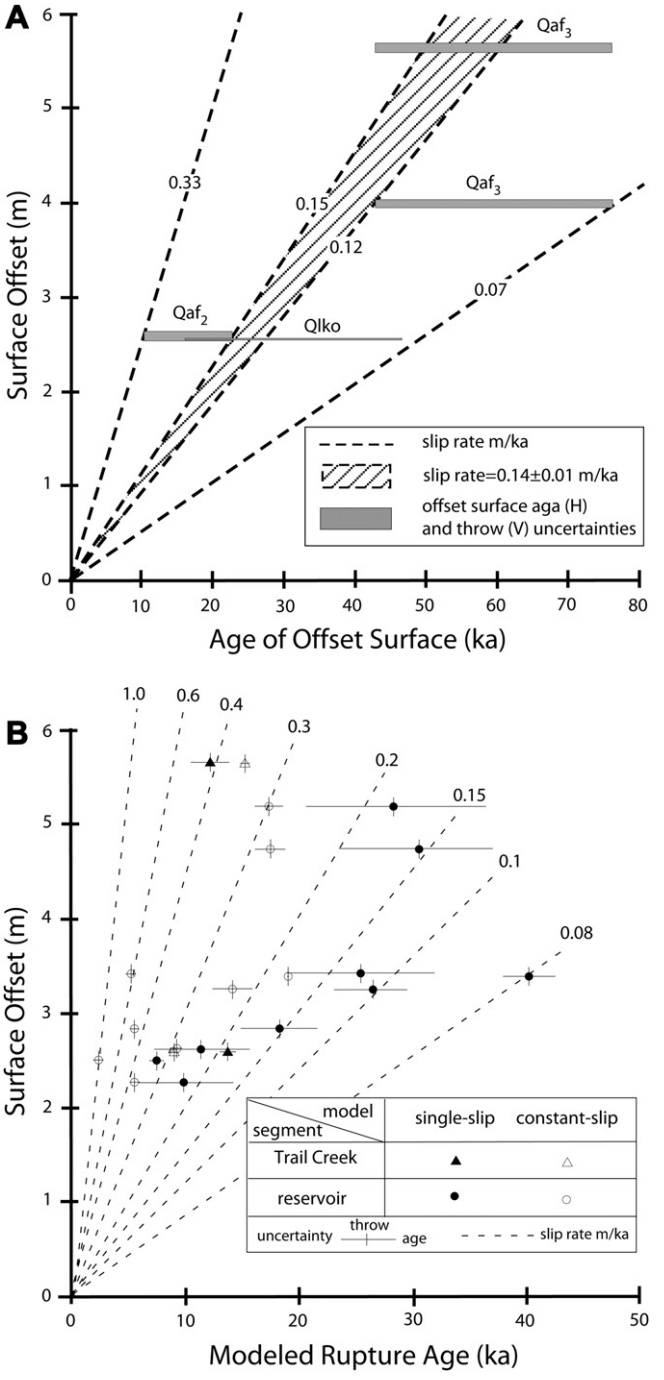

Fig. 9. A. Graph of measured scarp throw versus offset surface age. Bounding slip rates in m/ka that satisfy the data at the extreme uncertainties in age and throw. Shaded region bounds the range of nearly constant-slip rates satisfying the data. H-horizontal uncertainty in age, V-vertical uncertainty in throws. Unit symbols same as text. B. Graph of modeled rupture age versus throw by model and fault segment. The spectrum of slip rate contours shown satisfies the data.

The surface offset (fault throw) divided by the modeled rupture age is reported as the most likely long-term slip rate (Fig. 9B and Table 2A and B). For the Trail Creek segment the average slip rate from two scarp profiles using the single-slip rupture ages is 0.32 ± 0.24 m/kyr and using the constant-slip rupture ages is 0.33 ± 0.01 m/kyr. For the eastern sector of the reservoir segment the average slip rate is 0.24 ± 0.07 m/kyr from single-slip modeling and 0.58 ± 0.08 m/ka from the constant-slip algorithm. Calculated slip rates from the central sector are slower, with a single-slip average rate of 0.15 ± 0.04 m/kyr and a constant-slip average of 0.27 ± 0.02 m/kyr. Considering all nine profiles transecting the reservoir scarp yields an average single-slip rate of 0.18 ± 0.05 m/kyr, whereas using the younger constant-slip rupture ages predicts a faster rate of 0.44 ± 0.05 m/kyr (Table 2A and B). The average slip rate for the Lima Reservoir fault based on all profiles using both modeling protocols was 0.31 ± 0.06 m/kyr.

5. Discussion

5.1. Paleoseismology of the Lima Reservoir fault

Evidence for two Pleistocene or Holocene ruptures on each of the Lima Reservoir fault segments includes offset and dated surficial deposits and rupture age determinations from morphological fault scarp modeling. Overlapping single-slip and constant-slip rupture age uncertainties is taken as confirmation of a rupture along a given profile and the average age from both modeling methods is taken as the most likely age of the paleoseismic event. Each segment of the Lima Reservoir fault was active in the Pleistocene but only the reservoir segment was active in the Holocene (Table 2A and B). The Henry Gulch, Trail Creek, and reservoir segments are each cut by modern drainages. No fault trace has evidence of offset active stream deposits or knick points to suggest that the Lima Reservoir fault has experienced a large ground-rupturing earthquake in the last few millennia. The spatial pattern of rupture ages and the temporal overlap in activity on the Lima Reservoir fault segments suggests seismogenic linkage but may belie a physical connection at depth given the short strike length of the Trail Creek and reservoir segments and their wide surface separation (e.g. King et al., 1994; Peacock and Sanderson, 1994; Chery et al., 2001a, 2001b).

5.1.1. Henry Gulch segment

Earliest evidence of a Middle Pleistocene rupture of the Henry Gulch segment was provided by the minimum age of the oldest lacustrine sample from the Merrell locality, 50.27 ka (Table 1). The seismically induced debris flows of Qdfo that dammed Red Rock Valley preceded the deposition of the Merrell locality lakebeds so the rupture was >50 ka. The simplest interpretation is that this records an earthquake on the Henry Gulch segment because of its proximity to the dammed valley canyon and the height of the preserved Henry Gulch scarps at up to 5 m. A subsequent rupture of the Henry Gulch segment had to occur after deposition of ruptured Qaf_2 deposits (22.94–10.42 ka), bracketing the rupture to > 10 ka. But by the deposition of unit C at the Merrell locality, dated at 37.40–22.78 ka (Hill et al., 2005), a fluvial environment had returned to the canyon narrows of the ancestral Red Rock River. This facies change signals an absence of subsequent large earthquakes on the Henry Gulch segment necessary to again dam the valley <23 ka. Qlko deposits (31.43 ± 15.17 ka) may have persisted up valley from the Merrell locality until perhaps 16.26 ka. We interpret Qlko as correlative with the small lake and marsh deposits of Merrell unit B dated at 46.00–37.56 ka and the younger fluvial deposits of unit C. So field relations suggest renewed paleoseismicity on the Henry Gulch segment between 23–10 ka.

5.1.2. Trail creek segment

Profile TC-1 across the Qaf_3 surface on the Trail Creek segment has twice as much throw as the scarp across Qaf_2 on profile TC-3, yet the derived rupture ages are similar. This correspondence suggests an earlier Middle Pleistocene rupture of the Qaf_3 surface, prior to Qaf_2 deposition that has an age range of 22.94–10.42 ka, but subsequent to Qaf_3 deposition dated at 76.60–43.18 ka. This interpretation supports a Middle Pleistocene rupture of the Trail Creek segment > 43 ka. A younger Late Pleistocene rupture of the Trail Creek segment is confirmed by the overlapping uncertainties of the modeled rupture ages on offset Qaf_3 and Qaf_2 surfaces. The single and constant-slip model were 13.18 ± 2.27 ka and 12.15 ± 0.68 ka, respectively. The mean younger rupture age of the segment combining the results from both scarp morphologic models was 12.66 ± 1.48 ka (Table 2B).

5.1.3. Reservoir segment

The offset Qaf_3 surface along the central sector of the reservoir segment has a mean rupture age of 23.31 ± 6.70 ka averaging both sets of models, the 28.30 ± 10·74 ka from single-slip results and 16.32 ± 2.67 ka from constant-slip results and provides further evidence of younger Middle Pleistocene rupture of the Lima Reservoir fault (Table 2B). Along the reservoir segment, the average constant-slip rupture age of the eastern sector was 5.60 ± 1.34 ka and for the single-slip models was 11.62 ± 6.08 ka yielding a mean Holocene rupture age of 8.11 ± 4.10 for the segment. The western Centennial fault just across Centennial Valley also evidences Holocene activity (Bartholomew et al., 1987) but there is no compelling evidence of Holocene rupture of either the Henry Gulch or Trail Creek segments.

5.2. Slip rates

Slip rates calculated from individual scarp profiles quantify the pace of fault throw and vary by more than an order or magnitude from as fast as 1.09 ± 0.23 m/ka (profile R-4) for a constant-slip simulation to as slow as 0.08 ± 0.01 m/ka (profile R-10, Fig. 9B) for a single-slip model. No one slip rate will satisfy the range of rupture ages and fault throws for either the Trail Creek or reservoir segment profiles. The average Holocene slip rate on the eastern sector of the reservoir segment is faster than the average Pleistocene slip rate from either the Trail Creek segment or the central reservoir segment. Taken as a whole, our results suggest that the slip rates on the Lima Reservoir fault have been non-steady over the Pleistocene and Holocene and they appear to be increasing (Fig. 9B). For example, younger Qaf_2 surface offsets are associated with faster slip rates than older Qaf_3 offsets and younger rupture ages with faster slip rates than older ruptures. Uncertainty in the conclusion that slip rates are accelerating on the Lima Reservoir fault stems from the common observation that the shorter the observational window, the faster the slip rate estimates become. On average, the Pleistocene-Holocene slip rate on the reservoir segment is 0.31 ± 0.05 m/ka and on the Trail Creek segment is remarkably similar at 0.32 ± 0.13 m/ka. Considering all rupture ages from single-slip and constant-slip models, the average Pleistocene-Holocene slip rate on the Lima Reservoir fault is 0.31 ± 0.06 m/ka.

5.3. Regional kinematics

Recently, a horizontal GPS velocity discrepancy was measured across the boundary between the northern Basin and Range province and the Snake River Plain using data from 132 continuous and campaign site occupations from 1994–2007 (Chadwick et al., 2007; Payne et al., 2008). The seismically active Basin and Range province is moving southwestward at an order of magnitude faster than the

adjacent Snake River Plain. Contemporary seismicity is largely on extensional faults but the Centennial fault has also generated right-lateral strike-slip focal mechanisms. Bartholomew et al. (2002), reports both strike-slip and normal slickenlines on faulted soils from the reservoir segment trench. Payne et al. (2008), calculated contemporary slip rates of 1.72 ± 0.2 m/kyr along a diffuse "Centennial Shear Zone", a broad zone of dextral shear encompassing the northern Basin and Range and Snake River Plain boundary, a region including the Centennial Valley and the Lima Reservoir fault. Slip on the south-dipping Lima Reservoir fault, the north-dipping Centennial fault, and southwest-dipping accommodation zone between them are collectively consistent with right-lateral accommodation across the "Centennial Shear Zone" and compatible with the clockwise rotation of the northern Basin and Range documented by the GPS geodesy (Payne et al., 2008). The Lima Reservoir fault segments localize a portion of the "Centennial Shear Zone" and form a diffuse link between the Monument Hill fault segments along the western flank of the Red Rock Hills and the Centennial fault along the northern Centennial Mountains, accommodating the faster southwestward extension of the northern Basin and Range province relative to the adjacent Snake River Plain.

6. Conclusions

Results from mapping and morphologic scarp modeling have defined the paleoseismology of fault scarps rupturing the Henry Gulch, Trail Creek, and reservoir segments of the Lima Reservoir fault in southwest Montana. Offset Quaternary deposits and modeled ages of fault rupture provide compelling evidence that the Lima Reservoir fault ruptured the Henry Gulch segment in the Middle Pleistocene >50 ka and again between 23–10 ka. The Trail Creek segment ruptured >43 ka and at ~13 ka and the reservoir segment ruptured in the Middle Pleistocene ~23 ka and again in the Holocene ~8 ka. However, the Lima Reservoir fault has not experienced a large ground-rupturing earthquake in the last few thousand years. The young rupture ages and evidence of multiple large earthquakes on each segment indicates that this is a seismically active fault system. The pattern of ruptures and similarity of rupture ages amongst the Lima Reservoir fault segments suggests they are seismogenically linked. Slip rates on the Trail Creek and reservoir segments average ~0.3 m/ka but appear non-steady and increasing.

Acknowledgements

Funding for the project was provided by EDMAP Program of the National Cooperative Geologic Mapping Program of the US Geologic Survey under Contract Numbers 06HQAG0088 and 07HQAG0112 awarded to D. J. Anastasio. Thanks to UNAVCO for providing the GPS equipment and training, and L. D. Anderson and J. K. Troy for field assistance. This paper is an outgrowth of the M.S, thesis of C.N Majerowicz at Lehigh University. K. Pierce Jr. is thanked for introducing us to the field area and M.J. Bartholomew for sharing unpublished research results. N. Harkins is thanked for discussions on fault scarp diffusion modeling and time in the field. Editorial direction from W. Dunne and manuscript reviews by D. Lageson and J. Knott improved the manuscript.

Appendix. Supplementary data

Supplementary data associated with this article can be found, in the online version, at doi:10.1016/j.jsg.2010.08.012.

References

Avouac, J.P., 1993. Analysis of scarp profiles; evaluation of errors in morphologic dating. Journal of Geophysical Research, B, Solid Earth and Planets 98, 6745–6754.
Bartholomew, M.J., Stickney, M.C., Henry, J., 1987. Perspective 28 Years After the August 18, 1958 Hebgen Lake Earthquake: Montana Bureau of Mines and Geology open file report 193.
Bartholomew, M.J., Stickney, M.C., Wilde, E.M., Dundas, R.G., 2002. Late quaternary paleoseismites: syndepositional features and section restoration used to indicate paleoseismicity and stress-field orientations during faulting along the main Lima reservoir fault, southwestern Montana. In: Ettensohn, R.F., Rast, N., Brett, C.E. (Eds.), Ancient Seismites. Geological Society of America Special Paper, vol. 359, pp. 29–47. Boulder, Colorado.
Bartholomew, M.J., Greenwell, R.A., Wasklewicz, T.A., Stickney, M.C., 2009. Alluvial fans: sensitive tectonic indicators of fault-segmentation and tectonic regime partitioning along the Red Rock fault, southwestern Montana, USA. Northwest Geology 38, 41–66.
Birkeland, P.W., 1999. Soils and Geomorphology. Oxford University Press, New York.
Bucknam, R.C., Anderson, R.E., 1979. Estimation of fault scarp ages from a scarp–height–slope–angle relationship. Geology 7, 11–14.
Chadwick, D.J., Payne, S.J., Van Hove, T., Rodgers, D.W., 2007. Contemporary tectonic motion of the eastern Snake River Plain: a campaign global positioning system study. Tectonics 26, TC6005. doi:10.1029/2005TC001914.
Chery, J., Carretier, S., Ritz, J.F., 2001a. Postseismic stress transfer explains time clustering of large earthquakes in Mongolia. Earth and Planetary Science Letters 194, 277–286.
Chery, J., Merkel, S., Bouissou, S., 2001b. A physical basis for time clustering of large earthquakes. Bulletin of the Seismological Society of America 91, 1685–1693.
Dawers, N.H., Anders, M.H., 1995. Displacement-length scaling and fault linkage. Journal of Structural Geology 17, 607–614.
Di Bucci, D., Massa, B., Zuppetta, A., 2006. Relay ramps in active normal fault zones; a clue to the identification of seismogenic sources (1688 Sannio earthquake, Italy). Geological Society of America Bulletin 118, 430–448.
Fairbanks, R.G., Mortlock, R., Tzu-Chien, C., Cao, L., Kaplan, A., Guilderson, T.P., Fairbanks, T.P., Bloom, A.L., 2005. Marine radiocarbon calibration curve spanning 0–50,000 years B.P. based on paired 230Th/234U/238U and 14C dates on Pristine corals. Quaternary Science Reviews 24, 1781–1796.
Gile, L.H., Peterson, F.F., Grossman, R.B., 1966. Morphological and genetic sequences carbonate accumulation in desert soils. Soil Science 101, 347–360.
Haller, K.M., Dart, R.L., Machette, M.N., Stickney, M.C., 2000. Data for Quaternary Faults in Western Montana. In: U.S. Geological Survey's National Earthquake Hazard Reduction Program Project on United States Map of Quaternary Faults and Folds 229.
Hanks, T.C., Bucknam, R.C., Lajoie, K.R., Wallace, R.E., 1984. Modification of wave-cut and faulting-controlled landforms. Journal of Geophysical Research 89, 5771–5790.
Hanks, T.C., 2000. The Age of Scarplike Landforms from Diffusion-Equation Analysis. Quaternary Geochronolgy: Methods and Applications, pp. 313–338.
Harkins, N.W., Anastasio, D.J., Pazzaglia, F.J., 2005. Tectonic geomorphology of the Red Rock fault, insights into segmentation and landscape evolution of a developing range front normal fault. Journal of Structural Geology 27, 1925–1939.
Hill, C.L., Albanese, J.P., Dundas, R.G., Davis, L.B., Batten, D.C., Herbort, D.P., Huber, J.K., Mulholland, S.C., Feathers, J.K., Root, M.J., 2005. The Merrell Locality and Centennial Valley, Southwest Montana, Pleistocene Geology, Paleontology, and Prehistoric Archaeology. Technical Report to the Dillon Office. USDI Bureau of Land Management, Bozeman, MT, 166 pp.
Kenner, S.J., Simons, M., 2005. Temporal clustering of major earthquakes along individual faults due to post-seismic reloading. Geophysical Journal International 160, 179–194.
King, G.C.P., Stein, R.S., Lin, J., 1994. Static stress changes and the triggering of earthquakes. Bulletin of the Seismological Society of America 84, 935–953.
Lynch, J.C., Burgmann, R., Richards, M.A., Ferencz, R.M., 2003. When faults communicate; viscoelastic coupling and earthquake clustering in a simple two-fault system. Geophysical Research Letters 30, 1–4.
Majerowicz, C.N., 2008. Quaternary rupture history of the Lima Reservoir fault system, SW Montana. MS Thesis, Lehigh University, Bethlehem, PA 49 p., 1 plate.
Majerowicz, C.N., Anderson, L.D., Anastasio, D.J., Pazzaglia, F.J., 2007. Bedrock and Surficial Geologic Map of the Henry Gulch 7.5' Quadrangle. Montana Bureau of Mines and Geology, Beaverhead County, Southwest Montana. Open File Report 563, 19p. 1sheet, scale 1:24,000.
Majerowicz, C.N., Troy, J.K., Anastasio, D.J., Pazzaglia, F.J., 2010. Bedrock and Surficial Geologic Map of the Lima Dam 7.5' Quadrangle. Montana Bureau of Mines and Geology, Beaverhead County, Southwest Montana. EDMAP 7, 17p. 2sheet, scale 1:24,000.
Marco, S., Stein, M., Agnon, A., Ron, H., 1996. Long-term earthquake clustering; a 50,000-year paleoseismic record in the Dead Sea graben. Journal of Geophysical Research 101, 6179–6191.
Mattson, A., Bruhn, R.L., 2001. Fault slip rates and initiation age based on diffusion equation modeling: Wasatch Fault Zone and eastern Great Basin. Journal of Geophysical Research 106, 13739–13750.
McLeod, A.E., Dawers, N.H., Underhill, J.R., 2000. The propagation and linkage of normal faults; insights from the Strathspey-Brent-Statfjord fault array, northern North Sea. Basin Research 12, 263–284.

Nash, D.B., 1980. Morphologic dating of degraded normal fault scarps. Journal of Geology 88, 353–360.
Nash, D.B., 1984. Morphologic dating of fluvial terrace scarps and fault scarps near West Yellowstone, Montana. Geological Society of America Bulletin 95, 1413–1424.
Nash, D.B., 1986. Morphologic dating and modeling degradation of fault scarps. In: National Research Council, Studies in Geophysics — Active Tectonics. National Academy Press, Washington, DC, pp. 181–194.
Nash, D.B., 2005. SlopeAge II. University of Cincinnati.
Payne, S.J., McCaffrey, R., King, R.W., 2008. Strain rates and contemporary deformation in the Snake River Plain and surrounding Basin and Range from GPS and seismicity. Geology 36, 647–650.
Perry Jr., W.J., Haley, J.C., Nichols, D.J., Hammons, P.M., Pontoon, J.D., 1988. Interactions of Rocky Mountain foreland and Cordilleran belt in Lima region, southwest Montana. In: Schmidt, C.J., Perry Jr., W.J. (Eds.), Interaction of the Rocky Mountain Foreland and the Cordilleran Thrust Belt. Geological Society of America Memoir, vol. 171, pp. 267–290.
Peacock, D.C.P., Sanderson, D.J., 1994. Geometry and development of relay ramps in normal fault systems. Bulletin of the American Association of Petroleum Geology 78, 147–165.
Pierce, K.L., Coleman, S.M., 1986. Effect of height and orientation (microclimate) on geomorphic degradation rates and processes, late-glacial terrace scarps in central Idaho. Geologic Society of America Bulletin 97, 869–885.
Regalla, C.A., Anastasio, D.J., Pazzaglia, F.J., 2007. Characterization of the Monument hill fault system and implications for the active tectonics of the Red Rock valley, southwestern Montana. Journal of Structural Geology 29, 1339–1352.
Ritter, J.B., Miller, J.R., Enzel, Y., Howes, S.D., Nadon, G., Grubb, M.D., Hoover, K.A., Olsen, T., Reneau, S.L., Sack, D., Summa, C.L., Taylor, I., Touysinhthiphonexay, K.C.N., Yodis, E.G., Schneider, N.P., Ritter, D.F., Wells, S.G., 1993. Quaternary evolution of Cedar Creek alluvial fan, Montana. Geomorphology 8, 287–304.
Stein, R.S., 1999. The role of stress transfer in earthquake occurrence. Nature 402, 605–609.
Stickney, M.C., Bartholomew, M.J., 1987. Seismicity and late quaternary faulting of the northern Basin and range province, Montana and Idaho. Bulletin of the Seismological Society of America 77, 1602–1625.
Stickney, M.C., Haller, K.M., Machette, M.N., 2000. Quaternary Faults and Seismicity in Western Montana. Montana Bureau of Mines and Geology Special Publication 117. scale: 1:753,984.
Stickney, M.C., Lageson, D.R., 2002. Seismotectonics of the 20 August 1999 Red Rock valley, Montana earthquake. Bulletin of the Seismological Society of America 92, 2449–2464.
Stuiver, M., Reimer, P.J., Bard, E., 1998. INTCAL98 radiocarbon age calibration, 24,000-0 BP. Radiocarbon 40, 1041–1083.
Wallace, R.E., 1977. Profiles and ages of young fault scarps, north-central Nevada. Geological Society of America Bulletin 88, 1267–1281.
Walsh, J.J., Bailey, W.R., Childs, C., Nicol, A., Bonson, C.G., 2003. Formation of segmented normal faults: a 3-D perspective. Journal of Structural Geology 25, 1251–1262.
Wegmann, K.W., Zurek, B.D., Regalla, C.A., Bilardello, D., Wollenberg, J.L., Kopczynski, S.E., Ziemann, J.M., Haight, S.L., Apgar, J.D., Zhao, C., Pazzaglia, F.J., 2007. Position of the Snake River watershed divide as an indicator of geodynamic processes in the greater Yellowstone Region, western North America. Geosphere 3, 272–281.
Wells, D.J., Coppersmith, K.J., 1994. New empirical relationships among magnitude, rupture length, rupture width, rupture area, and surface displacement. Bulletin of the Seismological Society of America 84, 974–1002.